Computational Materials Science 84 (2014) 163–174

Contents lists available at ScienceDirect

Computational Materials Science

journal homepage: www.elsevier.com/locate/commatsci

Atomistic investigation on the structure–property relationship during thermal spray nanoparticle impact

Saurav Goel [a,*], Nadimul Haque Faisal [b], Vilma Ratia [c], Anupam Agrawal [d], Alexander Stukowski [e]

[a] School of Mechanical and Aerospace Engineering, Queen's University, Belfast BT95AH, UK
[b] School of Engineering, Robert Gordon University, Garthee Road, Aberdeen AB107GJ, UK
[c] Tampere University of Technology, Tampere Wear Centre, Tampere FI-33101, Finland
[d] Department of Business Administration, University of Illinois at Urbana Champaign, 61820, USA
[e] Institute of Materials Science, Darmstadt University of Technology, Darmstadt D-64287, Germany

ARTICLE INFO

Article history:
Received 20 September 2013
Received in revised form 13 November 2013
Accepted 2 December 2013
Available online 31 December 2013

Keywords:
Thermal spray coating
Molecular dynamics
Copper
Particle impact
Flattening aspect ratio

ABSTRACT

During thermal spraying, hot particles impact on a colder substrate. This interaction of crystalline copper nanoparticles and copper substrate is modeled, using MD simulation. The quantitative results of the impacts at different velocities and temperatures are evaluated using a newly defined flattening aspect ratio. This ratio between the maximum diameter after the impact and the height of the splat increases with increasing Reynolds numbers until a critical value is reached. At higher Reynolds numbers the flattening aspect ratio decreases again, as the kinetic energy of the particle leads to increasing substrate temperature and, therefore, decreases the substrate resistance. Thus, the particle penetrates into the substrate and deforms less.

1. Introduction

'Thermal spraying' is a standard term used for coating processes where the sprayed layer is first formed by fully or partially melting the material at a high or moderate temperature (e.g. arc, flame, plasma, high-velocity oxy-fuel, detonation spray) or at cold temperature (e.g. cold spray) and then molten/semi-molten droplets are propelled through a spraying gun on the substrate in the form of splats or lamella [1]. Over the years, thermal spraying has gained wide popularity to produce coatings (typically in the thickness range of 50–500 μm) to combat surface degradation of engineered components. Typical industrial examples of thermal spraying include defence, biomedical, marine, nuclear, chemical, automotive, aeronautical and mining [2]. Coating materials such as metals, ceramics and cermets in nanostructured/fine/conventional micron powder sizes are generally used in thermal spray processes. Representative examples include Al/Cu/Ag for electrical components, Cu for printing industries, Al_2O_3 for textile and automotive machinery parts, WC-Co based wear-resistant coatings for aero-engine parts, yttria stabilized zirconia (YSZ) based thermal barrier coatings for turbine blades, Ni-based corrosion resistant coatings for chemical reactors and hydroxyapatite $Ca_{10}(PO_4)_6(OH)_2$ coatings for orthopaedic implants. More recently, thermal spray processes have been used to prepare nanostructured coatings using microsized nanocrystalline powder particles [3].

The properties of coating such as wear resistance, oxidation and corrosion resistance, thermal conductivity, electrical conductivity and self-lubrication are highly dependent on the properties of the splat, which in turn depends largely on spray parameters. A thermal spray is normally carried out using the following steps:

(a) Particles are heated with a flame or an arc at a high temperature in the range of 3000–15,000 °C to melt them.
(b) Molten particles are accelerated in a gas stream (300–3000 m/s) and propelled at high velocity (50–1000 m/s) on the surface to be coated, and
(c) Partially or fully molten particles flatten while impacting the substrate surface (normal or inclined) in the form of disk-like splats or splashes, and subsequently cool down

Abbreviations: BCC, body centred cubic; CR, cooling rate; CNA, common neighbour analysis; DXA, dislocation extraction algorithm; *E*, activation energy; *Exx*, strain tensor in *x*, *y* and *z* direction; EAM, embedded-atom-method; FCC, face centred cubic; HCP, hexagonally close packed; HPPT, high pressure phase transformation; *K*, Sommerfeld parameter; LAMMPS, large-scale atomic/molecular massively parallel simulator; MD, molecular dynamics; NVE, micro-canonical ensemble; NVT, canonical ensemble; OVITO, open visualization tool; *R*, universal gas constant; Re, Reynolds number; μ_0, viscosity at the melting point; VMD, visual molecular dynamics; We, Weber number; YSZ, yttria stabilized zirconia.

* Corresponding author. Tel.: +44 028 90975625; fax: +44 028 90974148.
E-mail address: s.goel@qub.ac.uk (S. Goel).

http://dx.doi.org/10.1016/j.commatsci.2013.12.011
0927-0256/

(typically at 100–600 K/μs) and coalesce to yield the desired coating. In general, Sommerfeld parameter K ($K = We^{1/2}\,Re^{1/4}$ where We and Re are Weber number and Reynolds number respectively) is used to study the behaviour of the splat [4]. Without solidification on a dry surface, Sommerfeld parameter characterizes the droplet behaviour as follows [5]: $K < 3 \rightarrow$ rebound, $3 < K < 57.7 \rightarrow$ deposition, $K > 57.7 \rightarrow$ splashing.

While thermal spray processes for single particle elastic impacts provide some insights, the problem becomes complex when spraying involves a multitude of particles undergoing significant plastic deformation and fragmentation due to a number of simultaneously occurring processes such as the collapse of particle agglomerations, phase changes, adhesion and metallurgical transformations [6].

Macroscopic properties of thermal spray coatings such as hardness, porosity, surface roughness and mechanical strength depend on their microstructure. Previous studies have highlighted that the substrate's temperature with respect to Leidenfrost temperature influences the tribology between the liquid droplet and the substrate [5]. Overall, while research in the arena of thermal spray is progressing [7], there are still many unexplored areas which may lead to improvements in this technology. Apart from experimental approaches to study thermal sprays [8], modelling approaches are also evident in the literature i.e., computational fluid dynamics [9], Monte-Carlo simulation [10], smooth-particle hydrodynamics [11] and finite-element methods [12] have been applied to study thermal spraying processes. Analytical models of droplet solidification on flat surface have also been proposed, but they are only able to explain the phenomena for a limited range of materials/conditions [13,14]. Moreover, recent trends in thermally sprayed ceramic coatings show a shifted emphasis on producing coatings with nanostructures or finer microstructures [15], in order to make use of the potential properties of the thick coating materials. Thus, there is a need to understand surfaces, interlayers and interfaces at an atomistic level in the thermal spray process. Since the relationship among processing conditions, particle characteristics, and the resulting coating properties is highly nonlinear and might not be thoroughly revealed by experimental studies, atomistic modelling can play an important role in the design and operation of thermal spray processes. An accurate understanding of thermal spray coating requires an insight into the structural, dynamic, energetic and rheological aspects in an atomic framework rather than the continuum framework [16,17]. Advances in modern computation and extant literature in the field of solid particle impact mechanisms also indicate that atomistic modelling is an excellent approach to complement the experimental findings. Such modelling can provide a better understanding of the underlying momentum, heat-transfer and other important mechanisms, which in turn, may be used to guide parameter design of thermal spray processes. Moreover, understanding the variability of a thermal spray process in real-time is essential to fabricate coatings having deterministic finish. Molecular dynamics (MD) simulation is an intermediate tool to bridge the gap of first principles, macroscopic and finite element methods, and is the method of choice when the properties to be studied are observable within the time scale accessible to simulations.

Since MD provides higher temporal and spatial resolution and capability to examine a phenomenon within a range of few picoseconds to femtoseconds; it is an appropriate choice for this work. The pioneering work of Shimizu et al. [18] is the only reported MD work in this domain to the best of authors' knowledge. Shimizu et al. [18] developed the models of aluminium–aluminium spray system using simple approximations of the Morse potential function. Their work does not take into account the resulting topography of the splat below the substrate's surface which can also affect the flattening process. In contrast to their work, the current work reports results for a copper–copper system described by a relatively better potential energy function. Some of the key questions that are addressed through this paper are:

(a) In a copper–copper thermal spray system, does the flattening aspect ratio vary with Reynolds number? Which other factors affect the flattening aspect ratio?
(b) What is the relative importance of the impact velocity and the temperature of the impacting particles in influencing the deviatoric strain energy induced in the substrate?
(c) How do the intermetallic properties vary with the change in temperature and velocity of the impacting particles?
(d) What are the time scales involved in flattening and solidification of the splat?

The above questions motivate the development and implementation of MD simulations in the current work. Exploration and analysis of parameters affecting the microstructure of coatings (e.g. which factors affect stress distribution) [19,20], will help enhance understanding of the thermal spray processes.

2. MD simulation

In this work, the "Large-scale atomic/molecular massively parallel simulator" (LAMMPS) [30] was used to perform a series of MD simulations. VMD [31], OVITO [32], and the dislocation extraction algorithm (DXA) [21–23] were used to visualize and analyze the atomistic simulation data. The following paragraphs detail the model and the algorithm followed in this work.

2.1. MD simulation model

A schematic diagram of the thermal spray MD simulation model is shown in Fig. 1. Periodic boundary conditions were applied in both X and Z axes of the system. The atoms of the substrate were allocated into one of the three different zones: Newton atoms, thermostatic atoms and boundary atoms, while the impacting particles were allocated to the zone of Newton atoms. The boundary atoms were assumed to be fixed in their initial lattice positions, serving to reduce the boundary effects and maintain the symmetry of the lattice. Newton atoms were allowed to follow Newtonian dynamics (LAMMPS NVE dynamics), while atoms in an intermediate thin boundary layer were subjected to a thermostat (LAMMPS NVT dynamics) to dissipate the extra heat generated in the finite simulation volume. This consideration of boundary conditions ensures that the process of deformation is not affected by any artificial dynamics. It may be noted here that this work considers vacuum which although an unpractical consideration, is still a good assumption to discard the role of ambient air or gas in order to make a careful examination of the effect of droplet momentum and the consequent splat formation.

2.2. MD simulation inputs

There are two significant phenomena involved in a thermal spraying experiment in general [2]:

1. If the sprayed particle temperature is lower than (but close to) the melting temperature, a high impact velocity is sought.
2. At temperatures above the melting point, the viscosity of the liquid particle decreases significantly. The viscosity μ follows the relationship $\mu = \mu_0 \cdot \exp(E/RT)$ where E is activation energy and μ_0 is the viscosity at the melting point. Hence, a relatively lower velocity is needed.

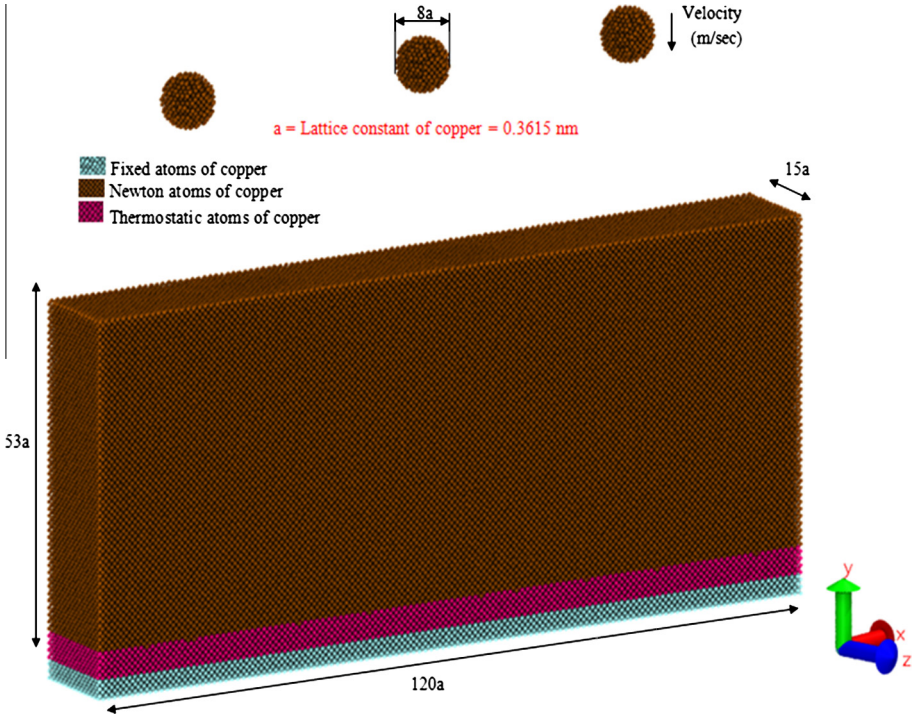

Fig. 1. Schematic of the MD simulation model.

In this work, copper was chosen as the work material which has a melting temperature of 1358 K. MD simulations were performed only up to 1000 K (below the melting point) to examine the role of impact velocity and to understand the high temperature resulting from the impact energy. An embedded-atom-method (EAM) potential energy function was used in this work to describe the interactions between copper atoms as it is more reliable than the Morse potential function [24].

Further details of these potential energy functions can be had from their respective reference. DXA was employed to examine the topography of the impact and to analyse the state of the deviatoric strain energy from atomistic data. A total of four trials were done: Trials 1, 2, and 3 comprise a full factorial experiment setup for particle velocity = (500, 1000, 1500) m/s and particle temperature = (500, 800, 1000) K, while Trial 4 is an exploratory trial for studying the effect of higher particle velocities (2000, 2500, 3000) m/s at a constant temperature of 1000 K. Hence, a total of twelve different parameter setups were used based on which results are presented in this work. In all twelve experiments, the substrate was kept at a constant temperature of 300 K, while nanoparticles with different velocities were sprayed on the substrate. This setup assures the validity and repeatability of experiments. For replication of results in the future, all the relevant parameters are tabulated in Table 1.

Fig. 2 shows a snapshot taken after the solidification of nano copper particles sprayed at an initial temperature of 1000 K with particles having velocities of 500 m/s, 1000 m/s and 1500 m/s (left to right) on a nanocrystalline copper substrate at 300 K. In this figure, brown coloured atoms[1] are copper atoms forming the crystalline FCC copper substrate while yellow coloured atoms are splats of the copper nanoparticles. A significant difference in the topography of the splats can clearly be seen from this snapshot. More details of the splat formation process and other comprehensive insights are detailed in the next section.

[1] For interpretation of color, the reader is referred to the web version of this article.

3. Results and discussions

3.1. Topography of the impacting particles

Fig. 3(a)–(d) shows snapshots at the end of simulation, after solidification of the splat. The figures highlight exclusively the topography and measurements of the splats. The dark line in the snapshots represents the top surface of the substrate and the vertical measurements below this line represent propagation of the splat in the substrate. Thus, the snapshot also shows the penetration depth, overall shape after flattening, and dimensions of the sub-surface penetration at different velocities and temperatures simulated. For clarity of detail, the cross sections of the splats were obtained by splicing the z–z section of the splat and switching off the substrate atoms in the software. z–z section was considered for inclusion of all the particles at once, although splicing of x–x was also symmetrical.

Fig. 3 shows that topography of the splat is significantly dependent on the impact velocity. At a lower velocity of 500 m/s, the topography is noticeably hemispherical, at 1000 m/s it is pyramidal, and at 1500 m/s, the degree of flatness above the substrate's surface increases and the topography resembles a mushroom. Furthermore, the diameter of the splat increases with an increase in impact velocity and so does the extent of the propagation of the splat in the sub-surface.

Comparing Fig. 3(a) and (b), it can be asserted that the post-impact typical shape of the splat does not change much with an increase in the particle temperature (except for the flattened diameter), although the dimensions of the splat changes. At a high temperature of 800 K, the flattening diameter is higher compared to that when the particle temperature is 500 K. This shows that the liquidity of the copper improves at 800 K.

A comparison of Fig. 3(b) and (c) show that the particle flattening diameter was less when spraying was performed at 1000 K, compared to that at 800 K, with the same velocity of 500 m/s. Thus the behaviour of liquidity with respect to the temperature is non-linear. Noticeably, the liquidity was found to improve further with higher velocities: the splat diameter is increasingly flattened at

Table 1
Process variables used in the MD simulation.

Details	Particle 1	Particle 2	Particle 3
Size of atomically smooth copper substrate	$120a \times 53a \times 15a$; Number of atoms: 3,88,800 $a = 0.3615$ nm;		
Size of one copper impacting particle	Diameter: $8a$; Number of atoms: 1048		
Inter-atomic potential function	Embedded-atom-method (EAM) [24]		
Substrate temperature (K)	300	300	300
Trial 1			
Particle velocity (m/s)	500	1000	1500
Particle temperature (K)	500	500	500
Trial 2			
Particle velocity (m/s)	500	1000	1500
Particle temperature (K)	800	800	800
Trial 3			
Particle velocity (m/s)	500	1000	1500
Particle temperature (K)	1000	1000	1000
Trial 4			
Particle velocity (m/s)	2000	2500	3000
Particle temperature (K)	1000	1000	1000
Crystal orientation of the substrate	(0 1 0)		
Targeted velocity of the particles	Orthogonal to the impacting surface		
Boundary conditions	*X* and *Z* boundaries were periodic type and atoms at the base were kept fixed		
Timestep (femtoseconds)	0.5		

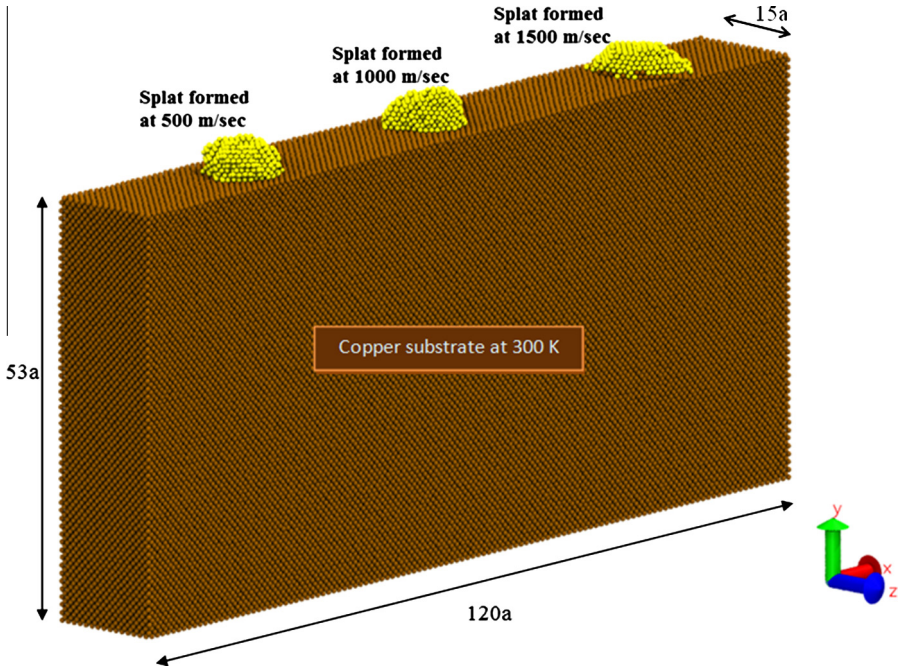

Fig. 2. Snapshot from the MD simulation showing splat formation at different velocities but at a common initial temperature of 1000 K of the copper particles.

higher velocities of 1000 m/s and at 1500 m/s. Also, the subsurface propagation appears to decrease with an increase in the particle temperature. The ratio of the height of splat below the surface to that above the surface is 74%, 62%, and 45% for the particle temperatures of 500, 800, and 1000 K respectively at the particle velocity of 1500 m/s.

In Fig. 3(d), a rapid increase in velocity from 2000 m/s to 3000 m/s can be seen to form random shapes of splat. In the subsurface, small crystallites of copper were observed to propagate in their pristine crystalline form (phase transformation is discussed in more details in Section 3.2.6). However, the degree of subsurface propagation can be observed to increase with increasing velocity of the particle, but the flattening diameter reduces with the increase in velocities above 2000 m/s. This shows that there exists a critical velocity beyond which the flattening diameter does not increase; instead, vertical propagation of the splat in the substrate has a more pronounced effect.

Escure et al. [5] observed that the diameter of alumina splats was smaller at a particle temperature of 300 K than that of 1000 K. In the current investigation, this phenomenon was found to occur only at higher impact velocities i.e. the splat diameter was observed to increase at higher impact velocities of 1000 m/s and at 1500 m/s but reduced with an increase in particle temperature when directed at lower velocities of 500 m/s. The fluidic

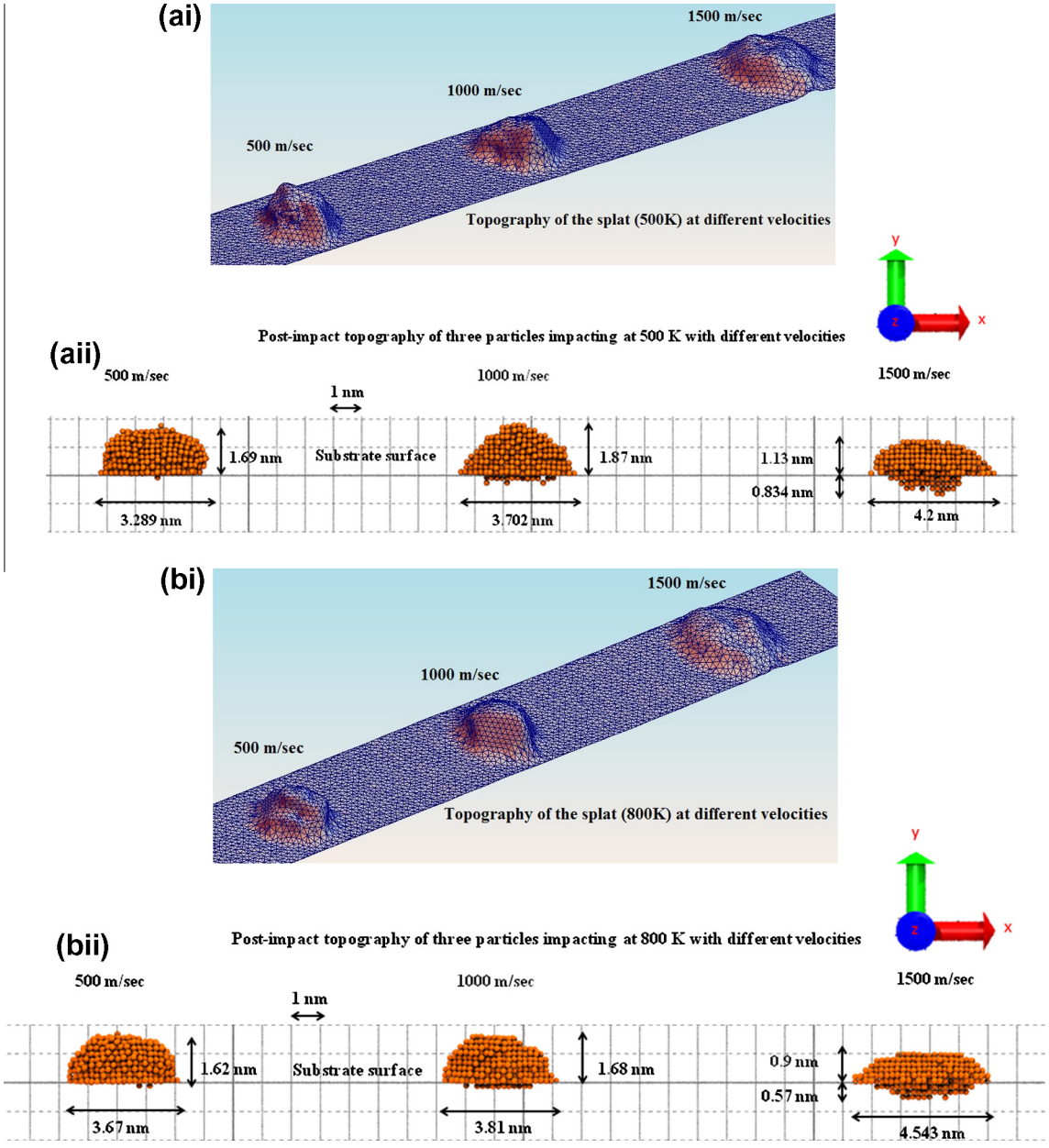

Fig. 3. Snapshot from the MD simulation using DXA algorithm to obtain meshed topography.

particles (at a temperature lower than melting point) are more viscous, and when they are directed at lower velocity, their flattening is obstructed by the inertial forces which need to be overcome. To overcome the inertial forces, a suitable and higher impact velocity is needed for better flattening. The kinetic energy of the sprayed particles gets transformed into separate components of work – viscous deformation, vertical sub-surface propagation into the substrate and surface energy. Also, the extent of the intermediate contact and thus the quality of the splat depends upon the impact pressure which in turn depends significantly on the contact surface. This also aligns with the fact that copper has a much larger thermal inertia (almost 10 times) than that of alumina.

3.2. Analysis of topography of the impacting particles

3.2.1. Flattening ratios

As a quantitative indicator, two parameters, flattening diameter ratio [18] and flattening aspect ratio are used in this work and their variation with the spray parameters is plotted in Fig. 4. These parameters are defined as follows:

$$\text{Flattening diameter ratio} = \frac{\text{maximum diameter post impact}}{\text{original diameter of the particle}} \quad (1)$$

$$\text{Flattening aspect ratio} = \frac{\text{maximum diameter post impact}}{\text{total height of the splat (above + below the substrate) post impact}} \quad (2)$$

The parameter of flattening diameter ratio was introduced in the early stages of thermal coating research to understand the flattening process quantitatively. However, this ratio does not take into account the extent of possible vertical (sub-surface) penetration into the substrate due to the impacting particle. Flattening aspect ratio is therefore introduced in this work as a more appropri-

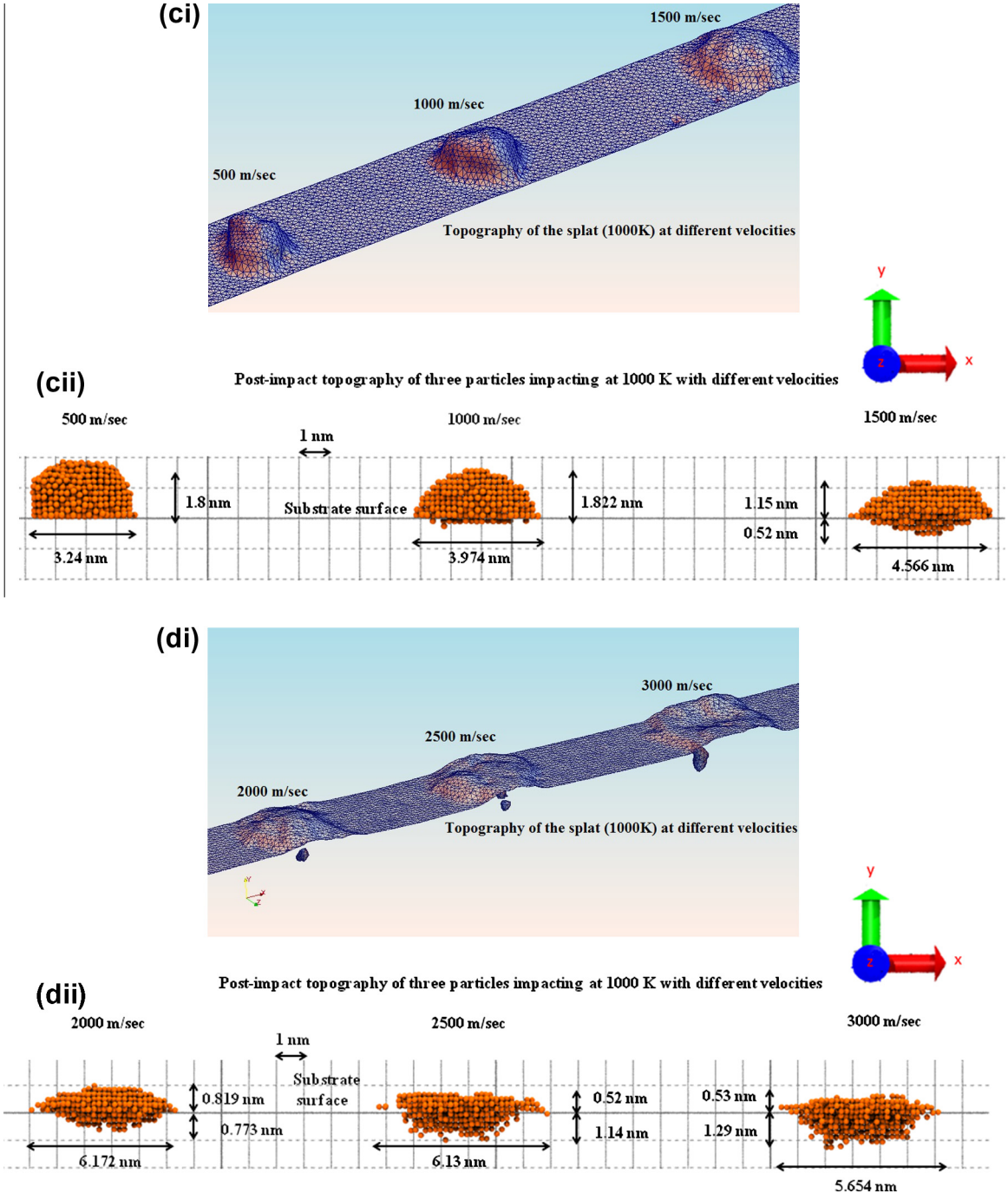

Fig. 3 (*continued*)

ate parameter to assess both vertical and horizontal deformations. Fig. 4 is a plot of the two ratios in line with the results tabulated in Table 2.

It can be seen from Fig. 4 that in contrast to the flattening diameter ratio, flattening aspect ratio shows a steady trend at temperatures up to 800 K and at velocities lower than 1000 m/s. This is because flattening aspect ratio considers the overall deformation, and unlike flattening diameter ratio it does not discard the effect of the sub-surface deformation. Since, the degree of sub-surface propagation of the splat is critical in influencing the overall flatness; the topographical measurements align with the above statements. It is therefore suggested that flattening aspect ratio is a more appropriate metric than the flattening diameter ratio to assess the overall deformation mechanisms. This parameter was found to change rapidly beyond the impact velocity of 1000 m/s up to 2000 m/s beyond which it decreases. This decrease in the ratio beyond a certain impact velocity cannot be suitably answered by flattening diameter ratio but flattening aspect ratio can comprehensively describes this phenomenon. A decrease in the flattening aspect ratio beyond a certain critical velocity and at a specific temperature is also in accordance with Fig. 3(d).

3.2.2. von Mises shear strain

It is useful to have a single characteristic strain value to describe the deviatoric degree of deformation and to examine the recrystallization behaviour. This value was calculated using the von Mises

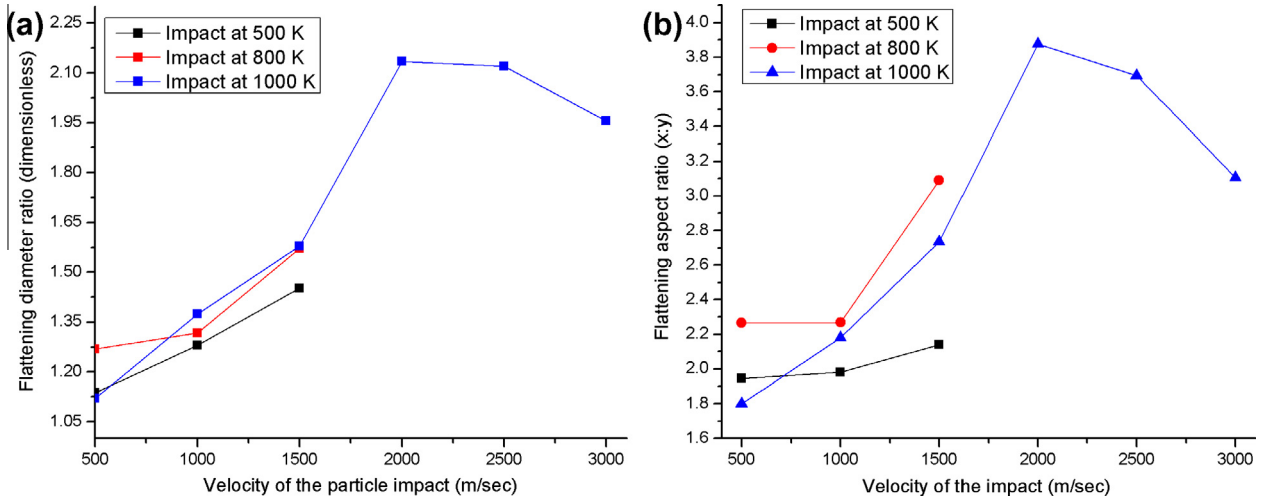

Fig. 4. Variation in the flattening ratios with respect to velocities of the particle impact when the particles were impacted at a preset temperature of 500 K, 800 K and 1000 K respectively.

shear strain. To quantify the plastic deformation of the atoms, an algorithm proposed by Shimizu et al. [25] was chosen. Atomic local shear strain (von Mises strain) for each atom i was computed by comparing the two atomic configurations (during impact and the starting configuration) using OVITO. This was accomplished by using a local deformation matrix $\boldsymbol{J_i}$ to first compute the local Lagrangian strain matrix as $\eta_i = \frac{1}{2}(J_i J_i^T - I)$, which was then used to compute the von Mises shear strain for each atom i. The von Mises shear strain η_i^{mises}, recognized as a good measure of the local inelastic deformation, can be expressed as follows:

$$\eta_i^{mises} = \sqrt{\eta_{yz}^2 + \eta_{xz}^2 + \eta_{xy}^2 + \frac{(\eta_{yy}^2 - \eta_{zz}^2) + (\eta_{xx}^2 - \eta_{zz}^2) + (\eta_{xx}^2 - \eta_{yy}^2)}{6}}. \quad (3)$$

Using this algorithm, the von Mises shear strains at different impact velocities for the same particle impact at an initial temperature of 500 K are shown in Fig. 5.

It can be seen from Fig. 5 that at higher impact velocities, maximum shear strain remains concentrated centrally underneath the sub-surface whereas at lower velocities, maximum strain is evident on the surface or with the peripheral atoms. This explains the difference in the patterns of recrystallization of the material impacting at different velocities. This also explains the reason for the existence of the residual strains in the sub-surface of the substrate, which results from a thermal spray system at higher spray velocities. Residual strains arising due to such phenomena have been demonstrated to initiate the failure of an orthopaedic implant, and a non-destructive method of neutron diffraction to characterize such residual strains in the substrate has also been proposed [26]. Hence, MD is useful to study such sub-surface phenomena's which would otherwise require sophisticated experimental setups to examine such details.

3.2.3. Effect of thermal diffusivity of copper

The process of reduced flattening after a certain critical temperature can also be studied from another perspective by analysing Figs. 6 and 7 together. Fig. 6 (adapted from [27,28]) shows that thermal diffusivity of copper reduces with an increase in temperature and drops suddenly at the melting point of copper (1358 K). Beyond 1358 K, the thermal diffusivity of copper becomes somewhat steady and increases with a gradual gradient. Fig. 7, which shows the data from MD simulation (the velocity of the atoms can be used to compute the local temperature of the atoms using the relationship between kinetic energy and temperature as $\frac{1}{2}\sum_i m_i v_i^2 = \frac{3}{2}Nk_bT$, where N is the number of atoms, v_i represents the velocity of ith atom, k_b is the Boltzmann constant ($1.3806503 \times 10^{-23}$ J/K) and T represents the atomistic temperature), shows that up to a temperature of 3600 K, the temperature induced in the substrate by the impacting splat remains lower than the instantaneous temperature of the splat itself. Consequently, the propagation of the splat into the substrate encounters a modicum of resistance. This makes the impacted zone of the substrate less viscous than the splat and hence the degree of deformation of splat is relatively more, which causes flattening of the splat. With increasing velocities, the impact energy induces sufficiently high temperature in the substrate more than the splat itself, and consequently, the vertical penetration of the splat directly into the substrate (without much flattening) becomes easier and thus flattening ratio decreases. Therefore, there exists a certain critical velocity at a specific temperature beyond which the flattening aspect ratio reduces and the impacting material's propagation in the substrate sub-surface increases.

3.2.4. Analysis with Reynolds number

In accordance with a previous suggestion [18], Reynolds number was also used to characterize the performance of the process. Reynolds number can be expressed as follows:

$$\mathrm{Re} = \rho V d/\eta \quad (4)$$

where V is the impact velocity (m/s), d is the diameter of particle (metre) before the impact, η is viscosity of copper at a particular temperature (considered as 3.8×10^{-3} Pa s at 1000 K [29]) and ρ is the mass density of copper which was calculated as:

$$\frac{\text{mass of one copper atom} \times \text{total number of atoms in one spray particle}}{\text{volume of one spray particle}} = 8602.53\ \mathrm{kg/m^3}.$$

It has been proposed that oxidation occurring during the process of splat formation is purely diffusion-controlled and is relatively low for particles with Reynolds number <20 whereas particles having Reynolds number >20 have a high degree of oxidation due to convection within the liquid droplet [30]. Fig. 8 plots the flattening aspect ratio and the flattening diameter ratio against Reynolds number of the impacting particles. Fig. 8 shows that beyond a certain critical Reynolds number, the flattening ratio (both flattening diameter ratio and flattening aspect ratio)

Table 2
Outcome obtained from the MD simulation under various impact parameters.

Impact parameters		Average von Mises stress induced in the substrate (GPa)	Peak local temperature induced in the substrate (K)	Peak local temperature of the particle post-impact (K)	Reynolds number	Flattening aspect ratio
Temperature (K)	Velocity (m/s)					
500	500	5	521	739	2	1.95
	1000	4.64	913	949	5	1.98
	1500	11.34	1770	1657	7	2.13
800						
	500	5.36	635	977	3	2.265
	1000	5.02	1145	1112	6	2.268
	1500	11.4	1563	1957	9	3.09
1000						
	500	4.08	715	1094	3	1.8
	1000	5.19	1028	1386	7	2.18
	1500	11.48	1540	1799	10	2.73
	2000	12.27	2163	2722	13	3.88
	2500	20.05	3519	3683	16	3.69
	3000	25.6	6463	4179	20	3.11

decreases because of the increased vertical propagation in the substrate as explained above. The maximum flattening ratio is realized when spray particles have certain Reynolds number (in the range of 10–16) and this range of Reynolds number can, therefore, be considered to be more amenable to a copper–copper spray system in cases where maximum flattening is desirable. An industrial application can be when a very fine finish coating is needed – so maximum flattening can give a thin layer of flat coating in fewer numbers of sprays, and this range of Reynolds number can be used for spraying at 1000 K. For thicker and rough coatings, less flattened particle spray system may be used.

3.2.5. Analysis of dynamics

In this section, the dynamic aspect of variation in the temperature of the splat and in the temperature induced in the substrate by the impacting particle is detailed in four selected cases. Fig. 9(a) and (b) shows the variation in the temperature in the splat and in the impact site of the substrate with respect to the simulation time when the spray was made at 500 K and 1000 K at a velocity of 500 m/s. Fig. 9(c) and (d) shows the variation in the temperature with respect to the simulation time when the spray was made at velocities of 1500 m/s and 3000 m/s both at a spray temperature of 1000 K. These cases represent four different subsets of high and low velocity and different temperatures. An interesting observation common to all four plots is that in every case, the temperature of the substrate reaches a peak value prior to attaining a peak temperature by the splat. This could most likely happen during the time when the impact energy is transferred by the splat to the substrate and then it requires a little bit of time for the splat to flatten. During this time, the temperature of the splat increases and attains a peak maximum value. Thus, the time frame between observing the two peaks of maximum temperature of the splat and of the substrate can be regarded as the flattening time. Careful observation revealed that this flattening time in all the cases was up to 2 picoseconds. Once the process of flattening completes, then the cooling of the splat and the substrate occurs.

The cooling of the splat is due to the heat conduction to the substrate. When the splat and the substrate (impacted by the splat) both reach a common equilibrium temperature, the condition of heat balance is achieved. The time from the completion of flattening to the time when the heat balance is attained (when the sprayed particles and the substrate site are in equilibrium) can be regarded as the cooling time or the time required for the solidification of the splat. For the configuration simulated in this work, cooling time was precisely noted to be about 30 picoseconds and was found to be independent of the velocity and the temperature of the spray particles. This is in contrast to earlier findings [2,5] which reported the time of few microseconds for splats of size of the order of millimetres – however, the splat size in the current work is of the order of nanometres.

Although cooling time and flattening time were observed to be the same in the simulated cases, the induced stresses in the substrate subsequent to the spray impact were different. The von Mises stress is a good indicator of shear deformation governing a shape change by activation of defect transport mechanisms, whereas hydrostatic stress associates itself with a change of volume leading to classical thermodynamic phase transition [16]. In the current simulation, von Mises stresses were found to vary significantly with respect to change in the velocity and temperature of the sprayed particle. The value of the von Mises stresses computed from the simulation in all the cases are plotted and shown in Fig. 10.

For impact velocities of up to 1000 m/s, the observed von Mises stresses induced in the substrate were rather low at levels of about 5 GPa. The trend of stress was however found to vary with respect to impact velocities (velocity more than 1000 m/s) when particles were sprayed between the temperatures 500 K and 800 K. Particles at 1000 K sprayed at higher velocity induced a significant variation in stress in the substrate in a range of 5–25 GPa depending on the velocity of the sprayed particle. Contrarily, particles having spray temperature of 500 K showed no significant differences in the stress induced in the substrate upon impact. It may be noted that there was a cross over in the von Mises stress (typically around 5 GPa) when the spray was made at 1000 m/s and the induced stresses at this velocity were found to be independent of the spray temperature.

3.2.6. Analysis of lattice disorder

In order to analyze the lattice disorder of the copper particles impacting upon the copper substrate after they have attained the equilibrium solidified state, cross sections of simulations were examined via common neighbour analysis [21]. For a material like copper (FCC), nearest-neighbours are calculated by their cut-off distance (r_{cut}). This cutoff distance for FCC materials is set halfway between the first and second neighbour shell as:

$$r_{cut}(\mathrm{FCC}) = \frac{1}{2}\left(\sqrt{1/2}+1\right)a_{\mathrm{FCC}} \cong 0.854 a_{\mathrm{FCC}} \tag{5}$$

where a_{FCC} is the lattice constant of copper which is 0.3615 nm.

Using this analysis, cross section of the splats were generated in the form of snapshots were shown in Fig. 11. The surface atoms of the splat and the substrate did not show any changes in the lattice

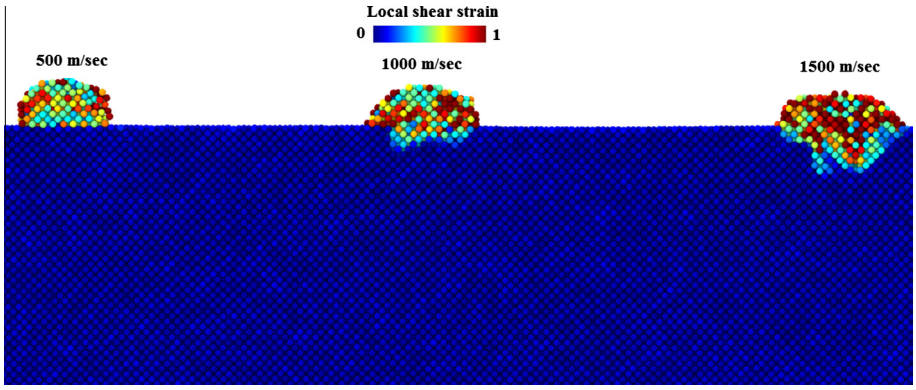

Fig. 5. Cross sectional view of the local atomic strain during impact made at an initial temperature of 500 K.

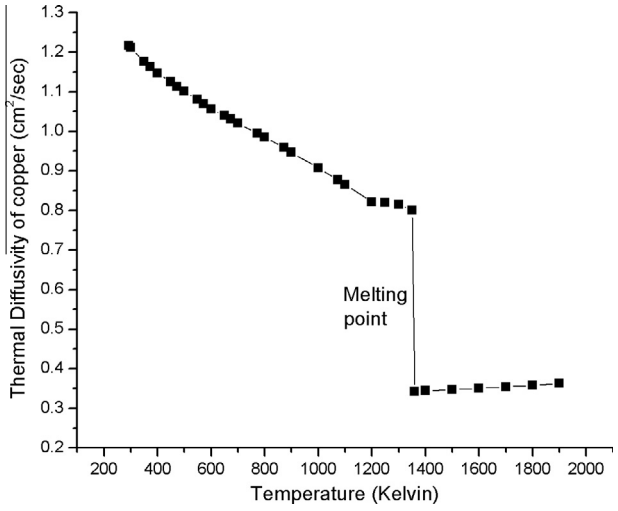

Fig. 6. Variation in thermal inertia of pure copper with respect to temperature – adapted [26,27].

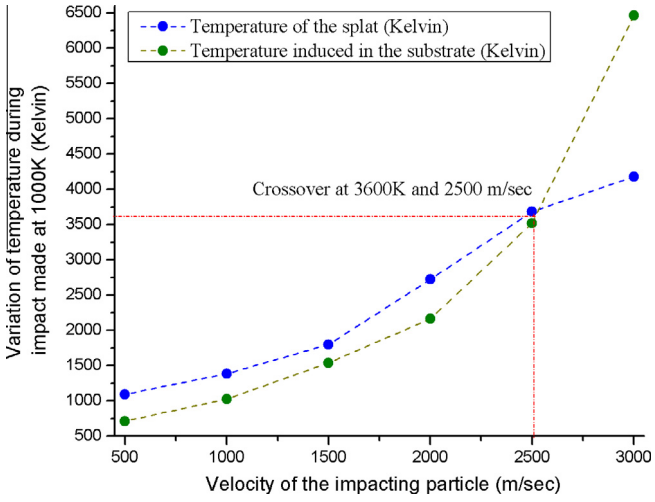

Fig. 7. Post-impact variation in the temperature of the splat and the impacted zone of the substrate with respect to velocity of the droplet during the spray at 1000 K.

disorder. However, spliced cross section (spliced using OVITO) revealed changes in the microstructure of copper nanoparticles after the spray.

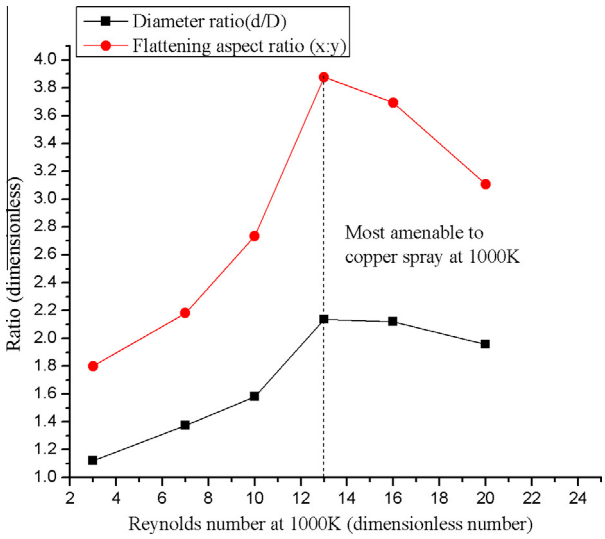

Fig. 8. Variation in the flattening ratios with respect to Reynolds number (sprayed at 1000 K).

Fig. 11 shows the results corresponding to 12 simulation trials at different velocities and temperatures. The impacts made at lower velocity (e.g. at 500 m/s) did not lead to an increase in the local temperature of the substrate or the splat up to melting temperature of copper and hence a large remnant of HCP copper atoms can be seen at lower impact velocities of 500 m/s independent of the spraying temperature. Particles sprayed at 500 K at low velocity of 500 m/s show a greater degree of formation of HCP copper. Spaepen [32] has presented an interesting list concerning requirement of energy via different modes for bringing structural changes in copper and suggested that HCP structure of copper can be created from the ground FCC structure merely by introducing stacking faults between every other stack of close-packed planes. The energy required for such transformation is predicted to be around 2.08×10^{-12} J as per the following equation:

$$\gamma_{SF} A_{(111)}/2 = 2.08 \times 10^{-12}\ \text{J} = 13\ \text{MeV} \quad (6)$$

where $A_{(111)} = 5.66\ \text{Å}^2$ is the area per atom in the close-packed plane and $\gamma_{SF} = 0.073\ \text{J/m}^2$ is the stacking fault energy which can be determined from the separation of partial dislocations.

At an impact velocity of 1500 m/s and up to 1000 K temperature impact, no significant phase change (either in the splat or in the subsurface) was observed which is likely due to melting and rearrangement of atoms. Also, up to an impact velocity of 1500 m/s sub-surface deformation was not evident, in contrast to the

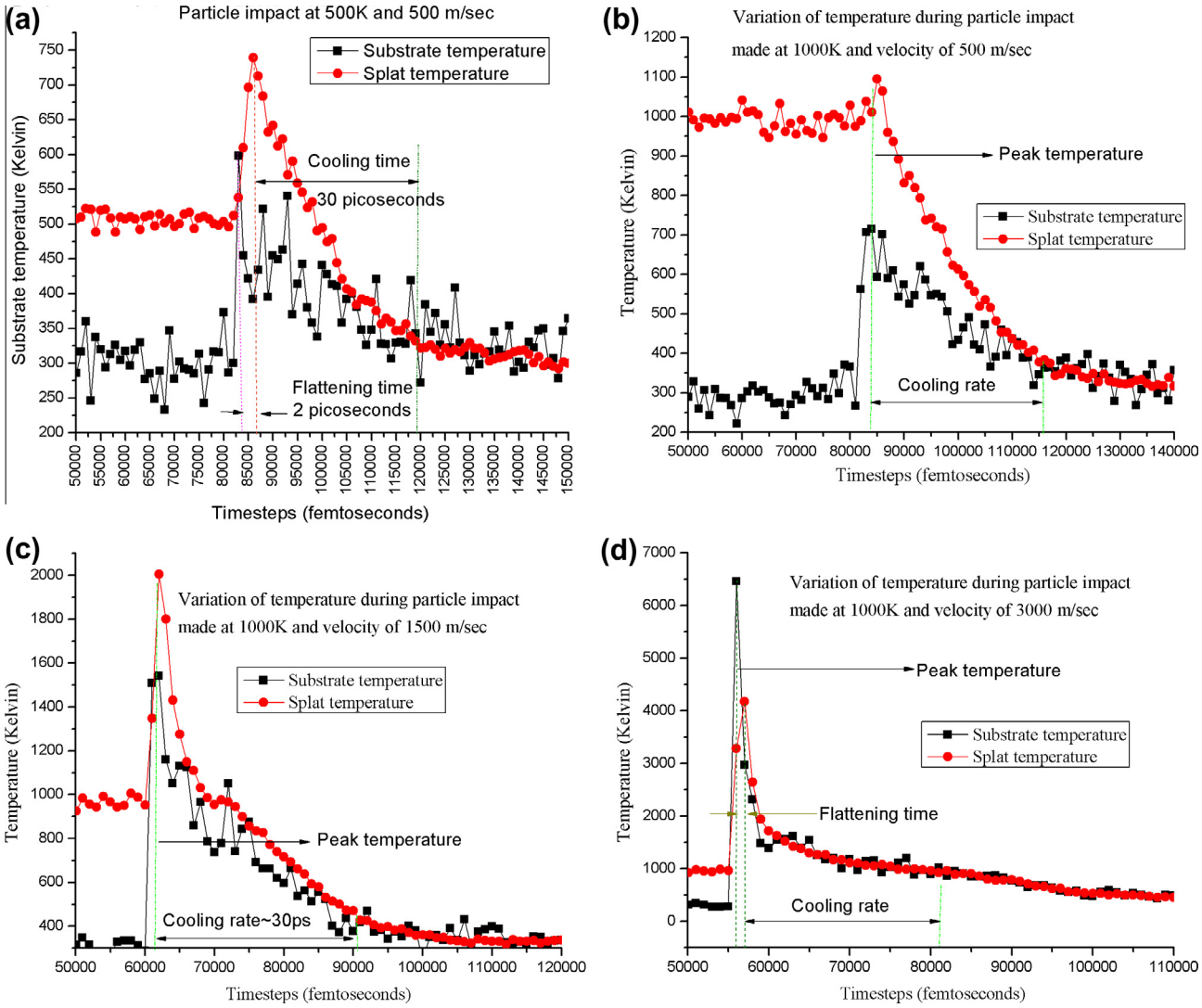

Fig. 9. Temperature variation in the splat and in the impacted site of the substrate with respect to time in selected cases.

impacts made at velocities above 1500 m/s at an impact temperature of 1000 K. Particularly at the impact velocity of 3000 m/s; there were some apparent sites in the substrate having HCP copper. This shows that at extremely high impact velocities microstructure of the sub-surface is liable to undergo a phase transformation.

Fig. 12 shows a 3D plot of flattening aspect ratio varying with particle velocity and temperature. A velocity of 2000 m/s and impact temperature of 1000 K showed the highest degree of flattening aspect ratio (up to 3.88) for the range of parameters investigated in this work.

3.2.7. Comments on the future research directions of the structure–property relationship

Due to the complex nature of the thermal spray process, modelling has been playing a key role in providing some key insights for process design and operations. The relationships among processing conditions, particle characteristics, and the resulting coating properties are nonlinear and might be difficult to be unravelled by the experimental studies alone (e.g. [5–7]) Detailed information on the atomic level changes leading to changes observed at macroscale can appropriately be obtained by MD simulation and the effect of temperature and velocity can be determined more precisely. In this work, relatively simpler spray system of copper–copper particle was simulated to obtain a better understanding of particle recrystallization and solidification, and deformation mechanics and topography of the impacting particles.

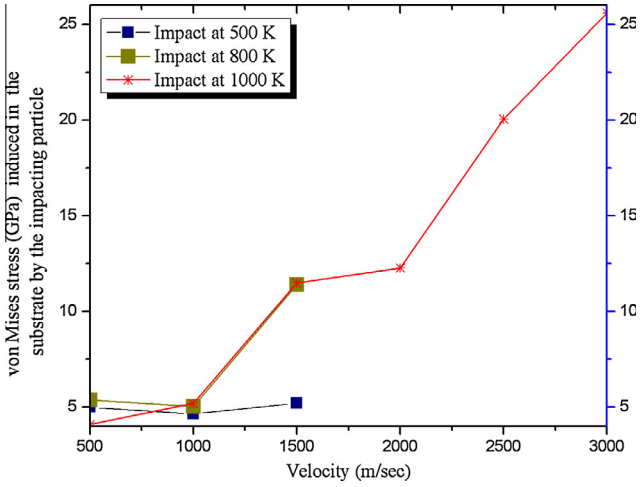

Fig. 10. Variation in the von Mises stresses induced in the substrate due to the impact.

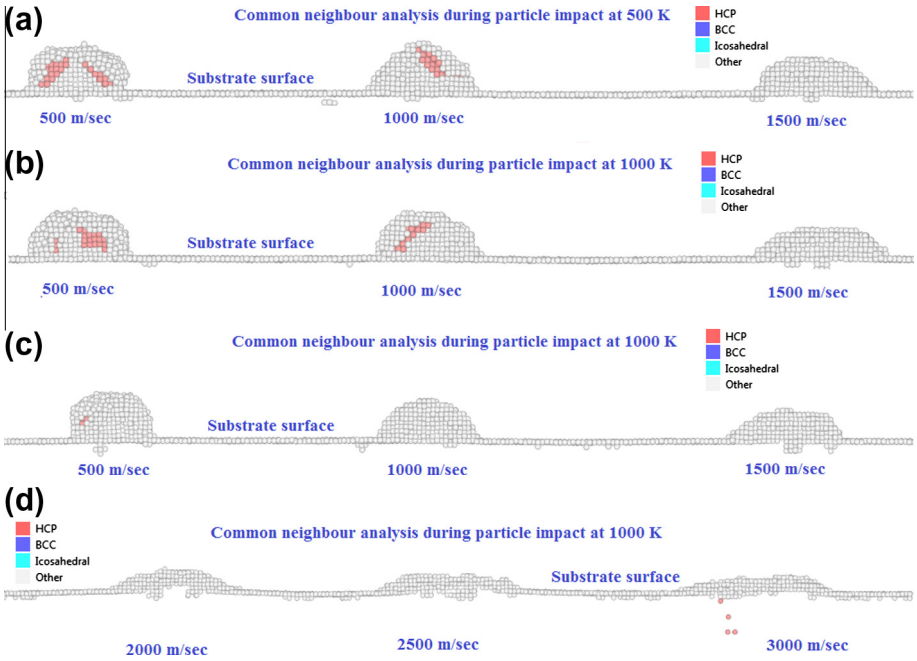

Fig. 11. Snapshot from the MD simulation showing cross sectional view of the splats at different velocities and at different temperatures in light of the induced lattice deformations monitored through common neighbour analysis (with cut off radius 3.08 Å) [31].

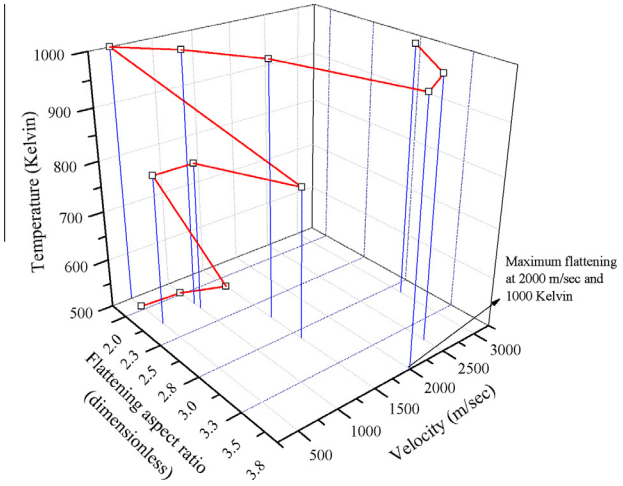

Fig. 12. 3D-plot of the variation in flattening aspect ratio with respect to velocity and temperature of the impacting particle.

Using state-of-the-art methods to examine the physical mechanisms involved in the impacting behavior and structure–property relationship, it can be suggested that the consecutive layer deposition of particles can better be understood by understanding individual particle impacts. The particle–surface interaction mechanism and its relation to Reynolds number can offer information on the quality of the coating through its response to shock heating. As a general practice, engineering components are thermally sprayed in a continuous multilayer mode with cooling; therefore there is an opportunity for developing richer theoretical models for single or multiple particle impact in conjunction with actual spraying tests, so as to identify cohesive and adhesive strength, hardness and residual stresses.

4. Conclusions

In this study, MD simulation has been used to reveal the deformation mechanics and for parameter optimisation of a copper particle based thermal spraying system for an atomically smooth copper substrate. A key finding was that a combination of the impact velocity of 2000 m/s and impact temperature of 1000 K is more amenable for smoother deposition. Based on the foregoing discussion, following other conclusions can be drawn:

1. An automated dislocation extraction (DXA) algorithm was used to explicitly study the topography and measurements of the splats such as measurement of penetration depth, overall shape after flattening and dimensions of the sub-surface penetration at different velocities and temperatures. It was found that the topography of the splat depends significantly on the impact velocity. At a lower velocity of 500 m/s, the topography was noticeably hemispherical, at 1000 m/s it was pyramidal, and at 1500 m/s, it attained the shape of a mushroom. The diameter of the splat increases with an increase in impact velocity and so does the extent of the propagation of the splat in the sub-surface.
2. In line with theoretical predictions, increasing flattening was observed with an increase in spray temperature from 500 K to 800 K but while increasing the spray temperature to 1000 K the flattening diameter *reduced* at a lower velocity of 500 m/s. The fluidic particles (at temperature lower than melting point) are more viscous and when they are directed at lower velocity, they cannot flatten much due to the inertial forces.
3. Flattening aspect ratio (introduced in this work) was found to scale up with the Reynolds number of the spray particles to a critical regime beyond which it reduced unexpectedly. Lower velocity causes lesser flattening, but flattening reduces with an increase of velocity above 2000 m/s on account of increased vertical propagation in the substrate.
4. Flattening time and cooling time were observed to be in few picoseconds i.e. 2 picoseconds for flattening and 30 picoseconds for cooling of the splat.
5. The von Mises stresses induced in the substrate by the spray (up to 6 GPa) were found to be independent of the spray temperature for lower velocities (up to 1000 m/s) and for lower spray temperature of 500 K. The von Mises stresses increase significantly at higher velocities beyond 500 K.

6. Common neighbour analysis revealed the formation of HCP phase of copper entrained in the splats and not in the substrate at relatively lower spray velocities and temperature when pristine FCC copper did not undergo melting at impact velocities up to 1500 m/s. Beyond 1500 m/s, the disorder gets induced in the substrate as the splat starts to undergo significant melting and recrystallization.

Acknowledgments

First author (SG) would like to acknowledge the funding support from J M Lessells travel scholarship from the Royal Society of Edinburgh (2013 RSE/J M Lessells Travel Scholarship) and International Research Fellowship account of Queen's University, Belfast. The authors would also like to acknowledge the use of University of Huddersfield Queensgate Grid and STFC Hartree Centre resources in undertaking this work.

References

[1] L. Pawlowski, The Science and Engineering of Thermal Spray Coatings, Wiley, 2008.
[2] P. Fauchais, A. Vardelle, M. Vardelle, M. Fukumoto, J. Therm. Spray Technol. 13 (3) (2004) 337–360.
[3] B.R. Marple, J. Voyer, J.F. Bisson, C. Moreau, J. Mater. Process. Technol. 117 (3) (2001) 418–423.
[4] C. Mundo, M. Sommerfeld, C. Tropea, Int. J. Multiphase Flow 21 (2) (1995) 151–173.
[5] C. Escure, M. Vardelle, P. Fauchais, Plasma Chem. Plasma Process. 23 (2) (2003) 185–221.
[6] N.H. Faisal, J.A. Steel, R. Ahmed, R. Reuben, G. Heaton, B. Allcock, Adv. Mater. Res. 13 (2006) 291–298.
[7] Foresight in surface engineering, U. Surface Engineering Committee of the Institute of materials, (Ed.), October 2000.
[8] C. Lin, C. Berndt, J. Therm. Spray Technol. 3 (1) (1994) 75–104.
[9] W.L. Oberkampf, Exp. Tech. 25 (3) (2001) 35–40.
[10] J. Mostaghimi, S. Chandra, R. Ghafouri-Azar, A. Dolatabadi, Surface Coat. Technol. 163–164 (2003) 1–11.
[11] M.Y. Zhang, H. Zhang, L.L. Zheng, Int. J. Heat Mass Transfer 51 (13–14) (2008) 3410–3419.
[12] R. Ghafouri-Azar, J. Mostaghimi, S. Chandra, Comput. Mater. Sci. 35 (1) (2006) 13–26.
[13] J.-P. Delplanque, R. Rangel, J. Mater. Sci. 32 (6) (1997) 1519–1530.
[14] M. Pasandideh-Fard, R. Bhola, S. Chandra, J. Mostaghimi, Int. J. Heat Mass Transfer 41 (19) (1998) 2929–2945.
[15] L. Pawlowski, Surface Coat. Technol. 203 (19) (2009) 2807–2829.
[16] S. Goel, X. Luo, R.L. Reuben, Tribol. Int. 57 (2013) 272–281.
[17] X. Luo, S. Goel, R.L. Reuben, J. Eur. Ceram. Soc. 32 (12) (2012) 3423–3434.
[18] J. Shimizu, E. Ohmura, Y. Kobayashi, S. Kiyoshima, H. Eda, J. Therm. Spray Technol. 16 (5–6) (2007) 722–728.
[19] R. Ahmed, H. Yu, V. Stoica, L. Edwards, J.R. Santisteban, Mater. Sci. Eng.: A 498 (1–2) (2008) 191–202.
[20] R. Ahmed, N.H. Faisal, R.L. Reuben, A.M. Paradowska, M. Fitzpatrick, J. Kitamura, S. Osawa, J. Phys.: Conf. Ser. 251 (1) (2010) 012051.
[21] A. Stukowski, Modell. Simul. Mater. Sci. Eng. 20 (4) (2012) 045021.
[22] A. Stukowski, K. Albe, Modell. Simul. Mater. Sci. Eng. 18 (8) (2010) 085001.
[23] A. Stukowski, V.V. Bulatov, A. Arsenlis, Modell. Simul. Mater. Sci. Eng. 20 (8) (2012) 085007.
[24] S.M. Foiles, M.I. Baskes, M.S. Daw, Phys. Rev. B 33 (12) (1986) 7983–7991.
[25] F. Shimizu, S. Ogata, J. Li, Mater. Trans. 48 (11) (2007) 2923–2927.
[26] R. Ahmed, N.H. Faisal, A.M. Paradowska, M.E. Fitzpatrick, K.A. Khor, J. Mech. Behav. Biomed. Mater. 4 (8) (2011) 2043–2054.
[27] P.H. Sidles, G.C. Danielson, J. Appl. Phys. 25 (1) (1954) 58–66.
[28] R. Gupta, Thermal diffusivity, in: Cryogenic data handbook, Brookhaven National Laboratory (BNL) UPTON: NY 11973, USA (Chapter 15).
[29] Hong-Xia GENG, G. Hao-Ran, Xian-Ying XUE, Ke YU, Jian-Tong LIU, Chin. Phys. Lett. 20 (7) (2003) 1102–1104.
[30] G. Espie, P. Fauchais, J. Labbe, A. Vardelle, B. Hannoyer, Oxidation of iron particles during APS: effect of the process on formed oxide. Wetting of droplets on ceramics substrates, in: ITSC 2001: International Thermal Spray Conference 2001, Singapore, 2001.
[31] G.J. Ackland, A.P. Jones, Phys. Rev. B 73 (5) (2006) 054104.
[32] F. Spaepen, Philos. Mag. 85(26–27) (2005) 2979–2987.

2013-12-31

Atomistic investigation on the structure-property relationship during thermal spray nanoparticle impact

Goel, Saurav

Elsevier

Goel S, Faisal NH, Ratia V, Agrawal A, Stukowski A, Atomistic investigation on the þÿstructure property relationship during thermal spray nanoparticle impact Materials Science, Vol. 84, March 2014, pp. 163-174

http://dx.doi.org/10.1016/j.commatsci.2013.12.011